Journal of Nanobiotechnology

RESEARCH Open Access

Modification of transvaginal polypropylene mesh with co-axis electrospun nanofibrous membrane to alleviate complications following surgical implantation

Tao Guo[1], Xuechun Hu[2], Zhe Du[1], Xiuqi Wang[1], Jinghe Lang[1], Jian Liu[2,3], Haiyan Xu[2,3*] and Zhijing Sun[1*]

Abstract

Background Surgeries for treating pelvic organ prolapse involving the utilization of synthetic mesh have been associated with complications such as mesh erosion, postoperative pain, and dyspareunia. This work aimed to reduce the surgical implantation-associated complications by nanofibrous membranes on the surface of the polypropylene mesh. The nanofiber of the nanofibrous membrane, which was fabricated by co-axial electrospinning, was composed of polyurethane as fiber core and gelatin as the fiber out layer. The biocompatibility of the modified mesh was evaluated in vitro by cell proliferation assay, immunofluorescence stain, hematoxylin-eosin (HE) staining, and mRNA sequencing. Polypropylene mesh and modified mesh were implanted in a rat pelvic organ prolapse model. Mesh-associated complications were documented. HE and Picro-Sirius red staining, immunohistochemistry, and western blotting were conducted to assess the interactions between the modified mesh and vaginal tissues.

Results The modified mesh significantly enhanced the proliferation of fibroblasts and exerted a positive regulatory effect on the extracellular matrix anabolism in vitro. When evaluated in vivo, no instances of mesh exposure were observed in the modified mesh group. The modified mesh maintained a relatively stable histological position without penetrating the muscle layer or breaching the epidermis. The collagen content in the vaginal wall of rats with modified mesh was significantly higher, and the collagen I/III ratio was lower, indicating better tissue elasticity. The expression of metalloproteinase was decreased while the expression levels of tissue inhibitor of metalloproteinase were increased in the modified mesh group, suggesting an inhibition of collagen catabolism. The expression of TGF-β1 and the phosphorylation levels of Smad3, p38 and ERK1/2 were significantly increased in the modified mesh group. NM significantly improved the biocompatibility of PP mesh, as evidenced by a reduction in macrophage count, decreased expression levels of TNF-α, and an increase in microvascular density.

Conclusions The nanofibrous membrane-coated PP mesh effectively reduced the surgical implantation complications by inhibiting the catabolism of collagen in tissues and improving the biocampibility of PP mesh. The

*Correspondence:
Haiyan Xu
xuhy@pumc.edu.cn
Zhijing Sun
sunzhj2001@sina.com

Full list of author information is available at the end of the article

incorporation of co-axial fibers composed of polyurethane and gelatin with polypropylene mesh holds promise for the development of enhanced surgical materials for pelvic organ prolapse in clinical applications.

Keywords Electrospinning technology, Pelvic organ prolapse, Transvaginal mesh implantation, Surgical complications

Background

Pelvic organ prolapse (POP) is a pelvic floor dysfunction resulted from weakened supporting tissues. The lifetime risk for women undergoing POP surgery is as high as 11.8–12.6% [1, 2]. Surgical intervention represents the most efficacious treatment, in which native tissue repair (NTR), laparoscopic sacrocolpopexy (LSC), and transvaginal mesh (TVM) implantation are the primary options available for managing POP. Compared to NTR surgery, both LSC and TVM procedures exhibit superior anatomical restoration and patient satisfaction rates, rendering the mesh implantation surgeries preferred approaches for treating POP [3, 4]. However, it has been noticed that the two approaches have raised international concerns regarding related complications post-surgery due to the utilization of synthetic meshes, including mesh erosion, postoperative pain, and dyspareunia [4–6]. A number of societies and associations across the world have advocated for restrictions on the mesh usage and operation indications due to these concerns [7]. Nevertheless, the mesh implantation is still increased because of its clinical advantages. Therefore, it is keen to develop technologies to facilitate safe applications of mesh in clinical practice.

The primary constituent of contemporary surgical meshes consists of polypropylene (PP) fibers. It has been recognized that the complications are largely attributable to the high modulus of PP fibers though PP is biologically inert. To mitigate complications associated with mesh implantation, some alternative materials have been explored to replace polypropylene (PP) mesh, including polyvinylidene, polylactic acid, polyurethane [8–10], or to modify the mesh surface with other polymers [11], however, no satisfactory one has been identified yet. In addition, fibroblasts, stem cells, or muscle cells have also been employed at the implantation site in studies [12, 13], unfortunately, this strategy has been fraught with ethical concerns, intricate procedures, low repeatability or limited cost-effectiveness.

In this work, a layered composite mesh was fabricated by depositing a kind of co-axial electrospun nanofibrous membrane on the clinically applied PP mesh. The electrospun fibers were composed of polyurethane as core and gelatin as shell. There are three main advantages for using this nanofibrous membrane as a modification for the PP mesh. Firstly, both gelatin and polyurethane possess favorable biocompatibility characteristics [14], rendering them suitable for application as surgical implant materials [15, 16]. Secondly, the mechanical properties of these nanofibers featuring a core-shell structure can be tailored by adjusting the ratio of the core and shell materials [17], enabling customization in accordance with clinical requirements. Thirdly, owing to their high porosity and high specific surface area, electrospun nanofibrous materials exhibit significant potential for the delivery of cells and drugs [18]. This characteristic compensates for the problem of PP fibers having a too simple structure and has the potential to be leveraged in the future for integrating cell therapy, drug therapy, and tissue engineering-based treatments for POP.

In this study, we observed that the electrospun membrane mitigated complications associated with PP mesh implantation in a rat model by enhancing surface biocompatibility and facilitating collagen deposition.

Materials and methods

Fabrication of polypropylene meshes deposited with nanofibrous membranes

Polyurethane (PU, YR-80P, Yantai Wanhua Polyurethane Co., Ltd., Yantai, China) or gelatin (Gel, V9000863, Sigma-Aldrich, Waltham, MA, USA) was dissolved in hexafluoroisopropanol to prepare 10% (g/mL) solutions. The two solutions were separately loaded into 5 mL syringes connected to the coaxial needle. The PU solution was used as the core component and Gel solution was the shell. The distance between the needle and the receiving plate was 15 cm, and the rotating speed of the receiver was 150 r/min. The voltage and flow rate of the two solutions were fixed at 20 kV and 0.0020 mm/s, respectively. Coaxial electrospinning was performed at room temperature with humidity of 50%. The collected nanofibrous membrane was vacuum dried for 48 h followed by heating at 120 ℃ for 4 h. The resulting nanofibrous membrane (NM) was attached to both sides of commercial polypropylene mesh (PP, Gynemesh™ TiLOOP, Ethicon, USA) and named as PP+NM. The PP meshes and PP+NM meshes were sterilized with ethylene oxide for subsequent assays.

Morphology characterization: The morphology of the PP mesh was observed by optical microscopy. The morphology of the nanofiber membrane was examined by scanning electron microscopy (SEM, ZEISS Gemini 300, Zeiss, Germany). The surface morphology of the material was examined using an environmental scanning electron microscope (ESEM, FEI, Netherlands, Quanta 200 F) under a vacuum of 130 Pa and at an accelerating voltage

of 20 kV. The distribution of nanofibers diameter was calculated by randomly counting and measuring 100 nanofibers in SEM images using the Image J software (National Institute of Health (NIH), Bethesda, MD, USA). The core-shell structure of the nanofibers was observed by transmission electron microscopy (TEM, HT7700, Hitachi, Ibaraki, Japan).

Water contact angle essay and uniaxial tensile test

The water contact angle of the NM was measured by the sessile drop method using a contact angle meter (DAS100, Kruss Scientific, Germany). A volume of 3 μL distilled water was gently dispensed onto the surface of NM to measure the contact angle. Three replicates were performed.

The elastic modulus of NM was measured using an electronic universal testing machine (SLBL, Shimadzu, Japan). The NM was cut into 100×15 mm rectangular test pieces and mechanically fractured at a 5 mm/min stretching rate. The elastic, strain, and force were recorded. Three replicates were performed.

Primary cell culture and animal experiments

This study has adhered to the laboratory animal welfare regulations and was approved by the ethics committee of Peking Union Medical College Hospital (no. JS-2240, 25/02/2020). Primary fibroblasts were derived from anterior vaginal wall tissues from patients with stage III or IV anterior vaginal wall prolapse according to the Pelvic Organ Prolapse Quantification (POP-Q). Vaginal wall tissues were collected from patients who underwent surgery for POP at Peking Union Medical College Hospital (PUMCH). Written informed consent was obtained from the participants. Briefly, specimens were cut into pieces smaller than 2 mm and then digested with 10 mg/ml collagenase type I (Sigma, St. Louis, MO, USA) at 37 °C for 2 h. The digestion mixture was filtered through a filter screen with 75-μm pore size and then centrifuged at 1000 rcf for 5 min. The cells at the bottom of the centrifuge tube were mainly fibroblasts. The cells were suspended in Dulbecco's modified Eagle's medium (DMEM; Gibco, Carlsbad, CA, USA) with 10% fetal bovine serum (FBS; Gibco) and cultured at 37 °C with 5% CO2. Cells at passage 3–7 were used in this study. PP+NM meshes or PP meshes were placed at the bottom of the 96-well or 6-well plates for in vitro assays. Each experiment utilized fibroblasts from three distinct patients as a biological replicate.

This study was in compliance with the NIH Guide for Care and Use of Laboratory Animals. Twenty-four 12-week-old female Sprague-Dawley rats (Charles River, Beijing, China) aged weighing 258±14 g were used in this study. Rats were raised at a temperature of 20–22 ℃, a relative humidity 50–70%, and a 12-hour day/night cycle. Food and water were supplied ad libitum. Our research group previously developed a POP rat model, which was employed for in vivo assays in this study [19]. Briefly, all the rats initially underwent ovariectomy (OVX) in the beginning. Two weeks after OVX, simulated vaginal delivery (SVD) was performed using a size 12 Foley catheter. A balloon injected with 2.5 ml 0.9% saline solution was inserted into the rat vagina and kept in for 4 h.

Implantation of the PP mesh or PP+NM mesh was performed two weeks after SVD. In a slightly moist, yet non-dripping state, the NM can adhere tightly to the surface of the PP mesh. The adhesion is sufficient to ensure successful completion of the surgical implantation procedures. In the experiment, the PP+NM mesh was gently wrapped with sterile gauze in a moist state prior to implantation surgery. During surgery, the PP/PP+NM mesh was sutured to the surrounding tissue for fixation. The incision site located at the midpoint of the lateral wall of the rat vagina was selected, as depicted in Fig. 1A. A 2 cm incision was made in the mucosa layer of the vaginal wall, and subsequently, either PP mesh or PP+NM mesh was placed in the sub-mucous layer. The mesh was sutured intermittently to secure it between the smooth muscle layer and connective tissue, followed by closure of the wound (Fig. 1B). Each group had 6 biological replicates at each time point.

Cell counting kit-8 assays

Primary fibroblast cells (4×10^3) were seeded into a 96-well plate (Corning) with trimmed PP mesh or PP+NM mesh in the wells. When the cell fusion reaches approximately 75%, cell counting kit 8 regent (CCK-8, Dojindo; Kumamoto, Japan) diluted with culture medium in 1:10 were added to each well and incubating for 45 min. Absorbance was measured at 450 nm using the Thermo Fisher Varioskan Flash (Thermo Fisher, CA, USA) microplate reader.

Immunofluorescent staining for F-actin

An actin-tracker red-555 kit (Beyotime, Shanghai, China) was used to visualize the filamentous actin (F-actin) of fibroblasts. Briefly, primary fibroblast cells on PP+NM were fixed using 4% paraformaldehyde for 15 min and washed with phosphate-buffered saline (PBS) containing 0.1% Triton X-100 three times. The working solution was then added and incubated for 60 min. After washing with PBS, cells were incubated with a 5 μg/mL DAPI solution for 5 min and washed with PBS three times. Cells were observed and photographed immediately using a fluorescence microscope (Nikon, Tokyo, Japan).

Hematoxylin-eosin (HE) staining

Primary fibroblasts cultured above the PP+NM meshes for 48 h or the PP+MN implanted POP rat vaginal wall

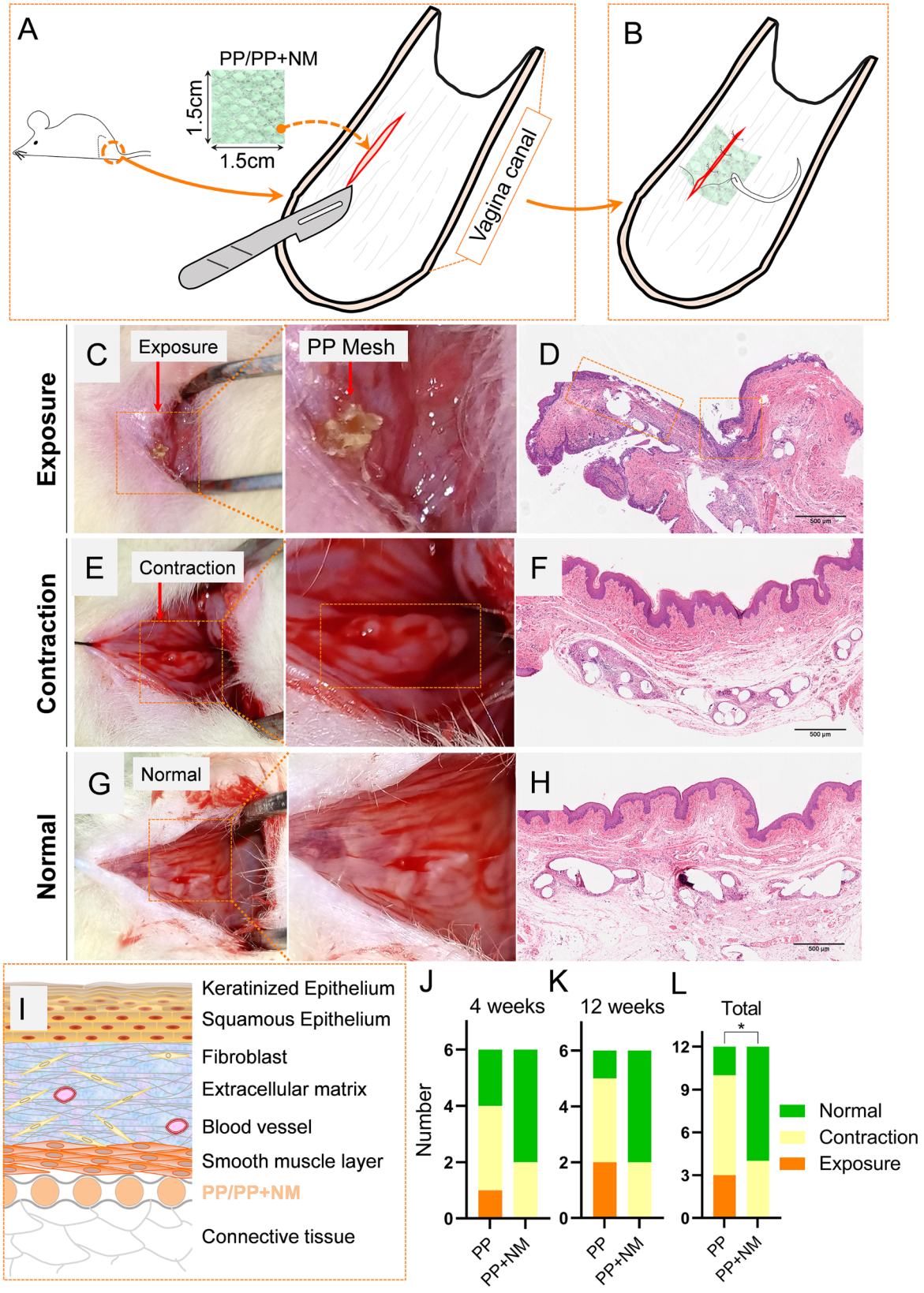

Fig. 1 In vivo evaluation of the modification effects on the complications of polypropylene (PP) mesh. Schematic diagram of the surgery process of implanting the mesh in rats (**A**-**B**). Representative images depicting the exposure, contraction, and normal states in a macroscopic view and hematoxylin-eosin staining (**C**-**H**). Schematic diagram of the structure of the vaginal wall and the position of the implanted mesh in rats (**I**). The number of exposures, contraction, and normal status at 4 weeks and 12 weeks (**J**-**K**). The combined data from two time points (**L**)

were fixed using 4% paraformaldehyde for 24–48 h. The dehydrated samples were embedded in paraffin, and then cut into sections (transection, 4 μm). After dewaxing, the slides were ready for HE staining. The slices were stained with hematoxylin for 5 min and rinsed with distilled water. After differentiation with alcohol hydrochloride for a short time, lithium carbonate was added for 2 min and then washed with distilled water. The slides were then stained with eosin solution for 50 s and rinsed with distilled water. After dehydration and treatment with xylene, the slides were covered with liquid mountant and coverslip. The slides were observed and photographed using a optical microscope (Nikon).

RNA-sequencing

Primary fibroblasts were seeded into a 24-well plate (Corning) with trimmed PP mesh or PP+NM mesh in the wells. The cells were cultured for 48 h. After the cell culture medium was removed, the cells were washed with PBS at 4℃ and the lysis buffer was then directly added. Isolation of total RNA was performed using the FastPure Cell/Tissue Total RNA Isolation Kit V2 (Vazyme Biotech, Nanjing China) according to the manufacturer's instructions. For RNA-sequencing, the NEBNext Ultra Directional RNA Library Prep Kit was used to prepare the library and the library was sequenced using the HiSeq PE150 platform (Illumina, San Diego, USA). GSEA analysis was performed using https://www.bioinformatics.com.cn (last accessed on 10 August 2024), an online platform for data analysis and visualization [20]. A *P*value under 0.05 and absolute log2 value of a fold-change greater than 2 were considered as statistically significant.

Picro-Sirius red staining

Slides were prepared as described above and were stained using Picro-Sirius red F3BA (Sigma, St. Louis, MO, USA) according to the manufacturer's instructions. The slides were observed and photographed using a polarization microscope (Nikon). Images were analyzed using Image-Pro Plus Version 6.0 software (Media Cybernetics, Silver Spring, USA). The red and yellow areas were identified as type I collagen and the green area was identified as type III collagen. The ratios of collagen I to collagen III were calculated for comparison among groups. They were observed and photographed using a polarization microscope (Nikon).

Immunohistochemistry

Slides were prepared as described above. The antigens were retrieved using citrate buffer and blocked by bovine serum albumin (Sigma). The slides were then incubated with specific antibodies at 4 ℃ for at least 12 h. The antibodies used in this study included ACTA2 (1:200, ABclonal; Wuhan China), matrix metalloproteinase 2 (MMP2) (1:100, ABclonal), MMP9 (1:100, ABclonal), tissue inhibitor of metalloproteinase-1 (TIMP1, 1:200, Invitrogen; Carlsbad, CA, USA), TIMP2 (1:100, ABclonal), F4/80 (1:4000, Proteintech, Wuhan, China), and TNF-α (1:1000, Proteintech). Horseradish peroxidase conjugated secondary antibodies were then incubated (Solarbio, Beijing, China) at room temperature for 30 min. Then, a DAB substrate kit (Solarbio) was used to visualize the sections. We used an optical microscope (Nikon) for photographing and the Image-Pro Plus Version 6.0 software (Media Cybernetics) for quantitative analysis of the images. We compared the percentage of positive area between groups. Microvascular density was assessed through regular immunofluorescent staining utilizing von Willebrand factor (vWF, 1:1000, Proteintech, Wuhan, China).

Western blot assays

Rat vaginal wall tissues at the mesh implantation site were collected and lysed in RIPA lysis buffer supplemented with protease and phosphatase inhibitors (Beyotime) at 4 ℃. The lysates were then centrifuged at 12,500 g for 15 min. Proteins in the supernatants were quantified by Bradford protein assay kit (Beyotime). Proteins were separated by 10% SDS-polyacrylamide gel (Invitrogen) and were transferred onto polyvinylidene difluoride (PVDF, Invitrogen) membranes by an iBlot® Gel Transfer Device (Invitrogen). Antigens were blocked by a blocking buffer for western blot (Beyotime). The membranes were then incubated on shaking table at 4 ℃ for at least 12 h with primary andibodies, including GAPDH (1:1000, Cell Signaling Technology, CST, Danvers, MA, USA), alpha smooth muscle actin (ACTA2, 1:1000, ABclonal), COL1 (1:2000, Proteintech), collagen-3 (COL3, 1:1000, Proteintech), TIMP1 (1:1000; ABclonal), TIMP2 (1:1000; ABclonal), MMP2 (1:1000; Abcam; Cambridge, UK), MMP9 (1:1000; Abcam), transforming growth factor-β1 (TGF-β1, 1:1000, ABclonal), P-Smad3 (1:1000, ABclonal), Smad3 (1:4000, Proteintech), P-p38 (1:1000, CST), p38(1:1000, CST), P-ERK1/2 (1:2000, CST), ERK1/2 (1:1000, CST), and Tubulin (1:1000, Solarbio). Horseradish peroxidase conjugated secondary antibodies (Solarbio) were then incubated at room temperature for 1 h. The immunoblots were visualized using an enhanced chemiluminescence (ECL) kit and photographed by gel imaging system (Tanon, Shanghai, China). Relative density of the immunoblot fragments was quantified using the Image J software.

Statistical methods

The software GraphPad Prism 9 software (GraphPad Software, Inc., USA) was used for statistical analyses and graphing. Descriptive data are presented as the means and standard deviations (SDs). Two-tailed Student's t

tests were used to compare mean differences between two groups. Fisher's exact test was used to compare the incidence of mesh complications between groups. Statistical significance was defined as $P<0.05$.

Results

Fabrication and characterization of polypropylene meshes with deposited nanofibrous membranes

The clinically utilized polypropylene (PP) mesh comprised an intricate network of interlaced polypropylene fibers (Fig. 2A-C). The diameter of the PP fibers was between 80 and 100 μm (Fig. 2D). Nanofibers are stacked together to form a nanofiber membrane, with diameters ranging from 700 to 1500 nm (Fig. 2F-H). The thickness of the nanofibrous membranes ranged from 100 μm to 200 μm. The nanofiber exhibited a composite structure comprising of a gelatin shell and an inner core of polyurethane (Fig. 2I).

In this study, the PP mesh was modified by attaching the nanofiber membrane to the surface (Fig. 2J). When observed using an environmental scanning electron microscope, NM in the moisture state was attached to the surface of the PP mesh (Fig. 2K). Under magnification, it was observed that NM adhered closely to the surface of PP fibers, clearly outlining their shape (Fig. 2L-M). Similarly, when observed from a lateral perspective, it was evident that NM demonstrated consistent adhesion to the surface of the PP mesh (Fig. 2N-P). The contact angle of the electrospun fibrous membrane (NM) was measured as 27.9±0.5 degree, showing that the surface was hydrophilic (Fig. 2Q). The Young's modulus of NM was determined to be 1.03±0.23 MPa, which exhibited a significantly lower value than that of PP mesh (~4.5 MPa) described in the literature [21].

Characterization of fibroblasts cultured on polypropylene mesh with nanofiber membrane (PP + NM) in vitro

The large pore size and smooth surface of the PP mesh (As shown in Fig. 2A-C) prevent direct cell culture, so we chose the cells on the cell culture plate as the control group. This cellular state serves as a representative model in laboratory settings and can be easily replicated by researchers. The growth rates of the two groups were similar during the initial three days, as determined by CCK-8 assays. However, on day 4, while cell proliferation stopped on the plate, cells in the PP+NM group continued to proliferate vigorously and had a significantly higher cell count compared to those on the plate ($P<0.001$, Fig. 3A). The morphology of the cells changed significantly on PP+NM (Fig. 3B-G). By immunofluorescent staining for F-actin, the fibroblasts was found to be extended, fusiform, and formed monolayer on the plate (Fig. 3B-D), while on PP+NM the F-actin fibers were more stressful, the cell morphology was diverse and the growth was multi-level superposition (Fig. 3E-G). H&E staining observations showed that the cells not only attached on the surface of the membrane, but also migrated into the NM interlayer, or even reached to the other side of the mesh, which indicated the nanofibrous membrane provided a three-dimensional space for cell growth (Fig. 3H).

In RNA-seq principal component analysis (PCA), a distinct separation was observed between biological replicates due to the utilization of fibroblasts from three different patients; however, the control group and the PP+NM group exhibited closer proximity to each other (Fig. 4A). The findings from PCA suggested that NM exerts a moderate influence on fibroblasts, leading to insufficient differences to significantly differentiate between the control and experimental groups in the PCA. There were 874 up-regulated genes and 1894 down-regulated genes, as dispicted in the volcano plot of Fig. 4B.

In the Gene Ontology (GO) analysis, differentially expressed genes were predominantly enriched in functional categories associated with extracellular matrix (ECM) regulation, chemokines, and signal transduction (Fig. 4C). Figure 4D-F illustrated the expression profiles of three distinct categories of genes of interest. As depicted in Fig. 4D, multiple collagen-encoding genes were significantly upregulated, whereas matrix metalloproteinases (MMPs) are primarily downregulated in the PP+NM group. The expression levels of genes involved in regulating or phosphorylating proteins related to the MAPK and TGF-β signaling pathways were markedly elevated (Fig. 4E). Additionally, gene expression linked to cell chemotaxis and inflammation was dispicted in Fig. 4F. In the KEGG enrichment analysis, significant alterations were observed in the TGF-β and MAPK signaling pathways (Fig. 4G), which aligns with our subsequent findings from animal experiments. In Gene Set Enrichment Analysis (GSEA), both ECM-related genes identified from GO enrichment analysis and MAPK signaling pathway-associated genes identified from KEGG enrichment analysis exhibited significant increases in the PP+NM group, indicating a potential role for NM in promoting ECM synthesis. Notably, despite chemotaxis and inflammation-related genes showed higher expression levels in the PP+NM group, no statistically significant differences were observed (Fig. 4H). This may be attributed to the inert nature of the PP mesh; although gelatin degradation enhances inflammatory responses, this effect does not reach statistical significance.

Modification effects of NM on the complications of implanted mesh in vivo

Figure 1 A-B illustrate the comprehensive procedure of mesh implantation, as detailed in the Materials and

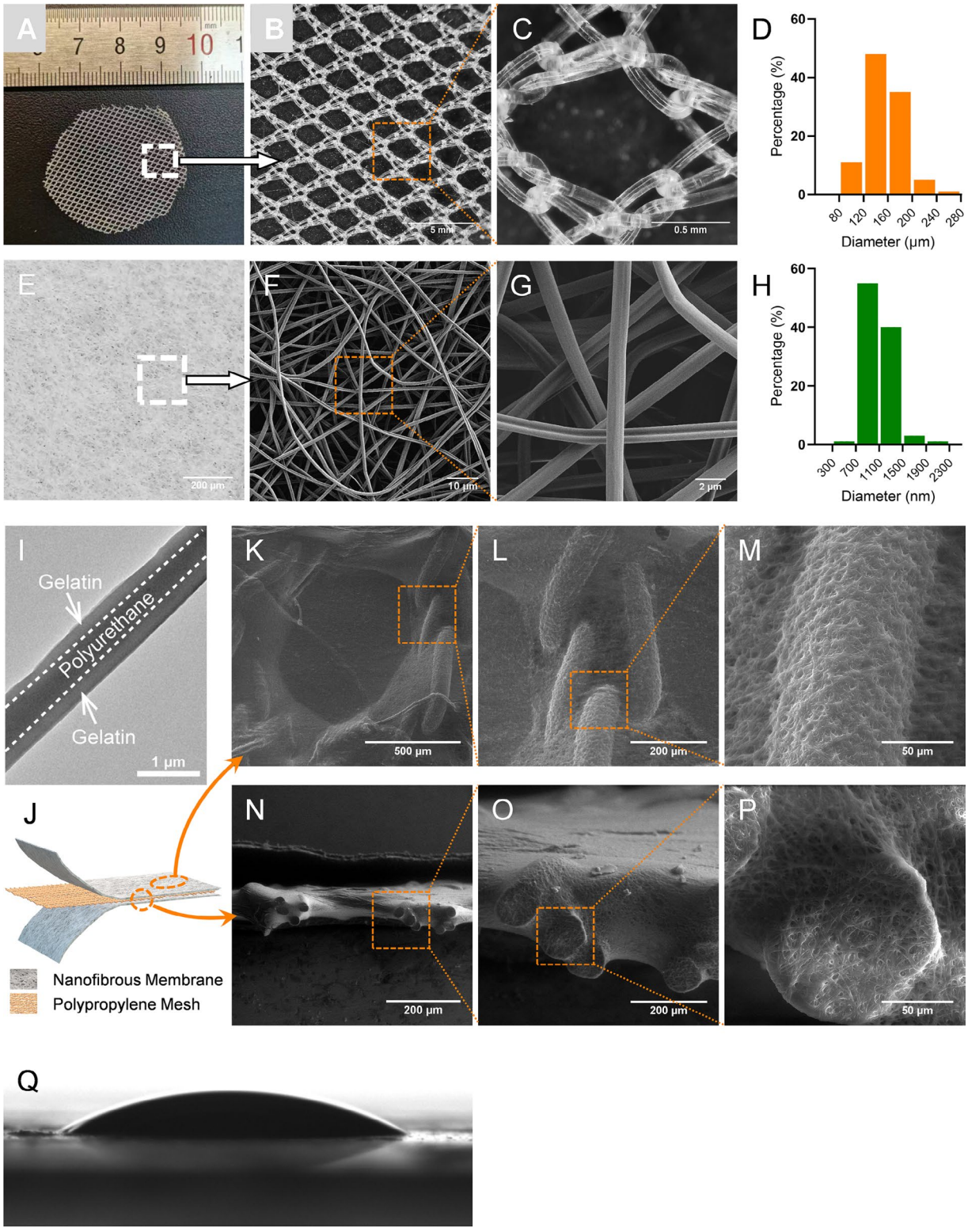

Fig. 2 Coating the polypropylene (PP) mesh with nanofibrous membrane (NM). Appearance of PP mesh under the macroscopic view (**A**) and an optical microscope (**B**-**C**). Diameter distribution of PP fibers (**D**). Appearance of NM under an optical micaoscope (**E**) and electron microscope (**F**-**G**). Diameter distribution of nanofiber (**H**). Explanation of the nanofiber structure with a electron microscope image (**I**). Schematic diagram for the construction of a PP mesh coated with NM (**J**). Images of the surface (**K**-**M**) and lateral (**N**-**P**) aspects of the PP mesh coated with NM examined using an environmental scanning electron microscope. Image of the water contact angle essay (**Q**). Scale bars in B and C are 5mm and 0.5mm, respectively. Scale bars in E, F, G, and I are 200um, 10um, 2um, and 1um, respectively. Scale bar in K is 500um. Scale bars in L, N, and O are 200um. Scale bars in M and P are 50um

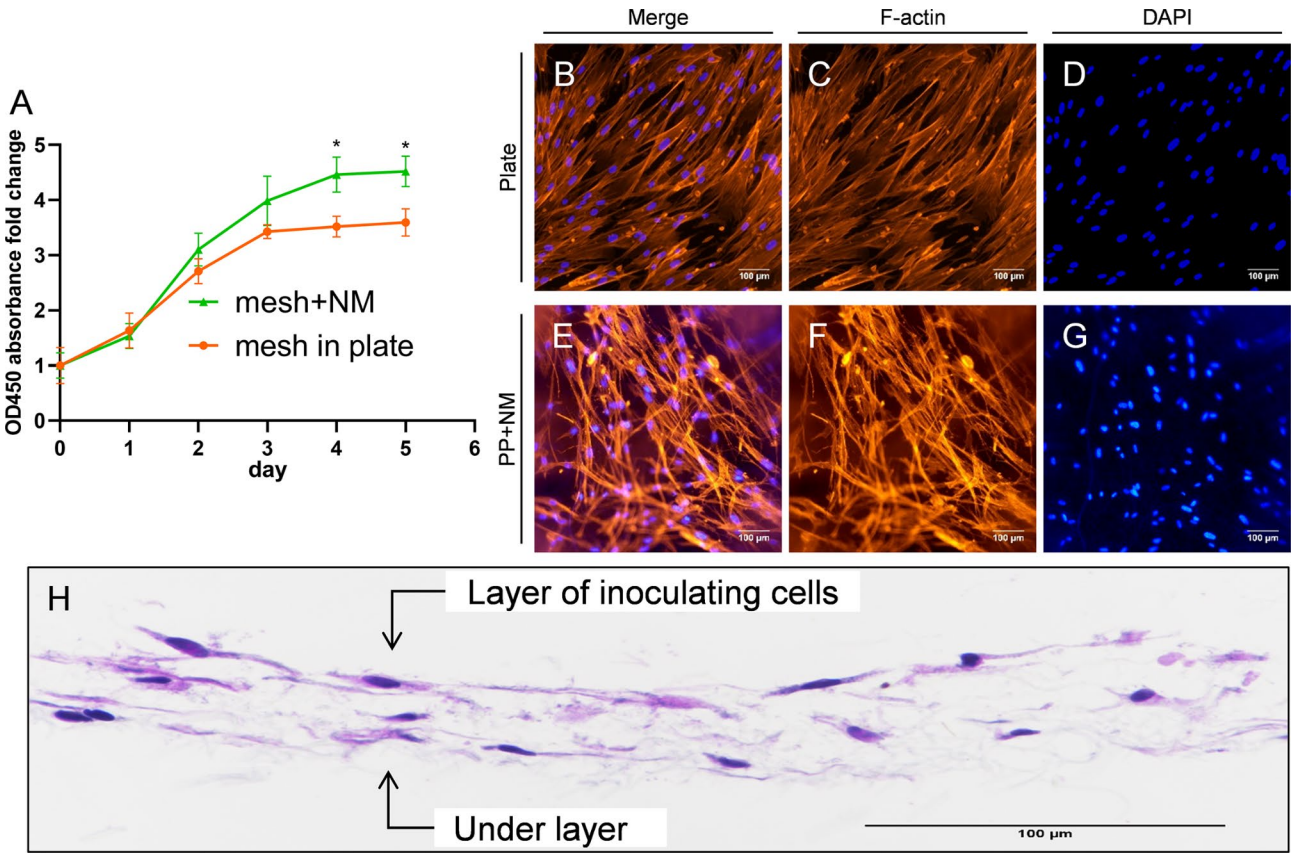

Fig. 3 Characterization of fibroblasts in vitro. CCK-8 assays for fibroblasts seeded on polypropylene mesh with nanofibrous membrane (mesh + NM) and mesh in plate (**A**). Immunofluorescence of F-actin for fibroblasts seeded on plate (**B**-**D**) and PP + NM (**E**-**G**). Hematoxylin-eosin staining for fibroblasts seeded on PP + NM (**H**). Scale bar in H is100um. * indicates $P < 0.05$

Methods section. Through observation and palpation, as used in clinical practice, the in vivo state of the mesh can be categorized into three distinct classifications: exposure, contraction, and normal [22]. The term "exposure" refers to the visualization of vaginal mesh through separated vaginal epithelium. "Contraction" denotes a reduction in size or shrinkage of the mesh, accompanied by raised and indurated mucosa upon palpation. In its normal state, the vaginal mucosa appears smooth without significant protrusion, with or without visible sign of appropriate healing at surgical incision sites. In Fig. 1 C-H, we presented representative images illustrating the three distinct mesh states examined in this study. Figures C, E, and G depicted the gross examination, while Figures D, F, and H illustrated the corresponding tissue morphology under HE staining. At the exposure sites (Fig. 1 C-D), the PP group exhibited wrinkling and an irregular arrangement of fibers, accompanied by a notable alteration in surrounding tissue structural integrity. The mesh penetrated through the epithelial layer, leading to its exposure. In regions where contraction occurs, although the mesh contracts and bulges outwardly, it remains confined within normal tissue layers (Fig. 1E-F). In a normal state, the mesh was between the smooth muscle layer and the connective tissue (Fig. 1G-H). We developed a schematic diagram to describe where the mesh was supposed to be when implanted into the rat vaginal wall (Fig. 1I).

As depicted in Fig. 1J-L, at 4 and 12-weeks post-implantation, in PP group, mesh exposure was observed in one case and two cases, respectively, while no exposure was observed in PP + NM group. The incidence of mesh exposure was significantly higher in PP group ($P = 0.024$). Additionally, the PP group exhibited a total of 7 instances of mesh contraction, whereas the PP + NM group demonstrated only 4 cases.

Changes of muscle fiber morphology and smooth muscle actin expression

In the PP group, the normal muscle fiber structure was disrupted, with the insertion of PP fibers into the midst of muscle fibers leading to their stratification (Fig. 5A-B). In the PP + NM group, the mesh was basically parallel to the muscle layer and did not invade the muscle layer (Fig. 5C-D). Although evident changes in muscle fiber morphology were observed, quantitative analysis

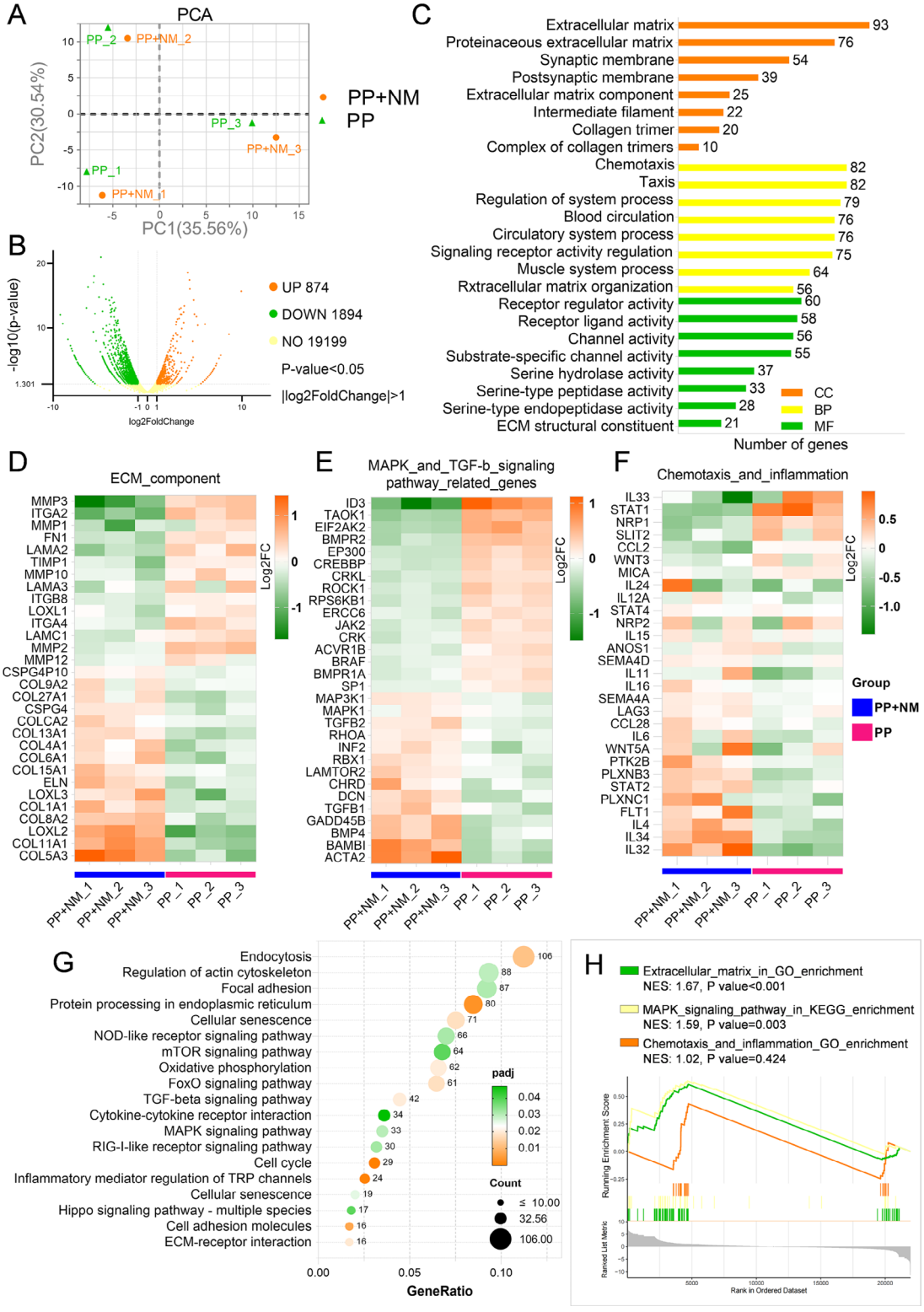

Fig. 4 Bioinformatic analysis of mRNA sequencing data from fibroblasts. The mRNA sequencing was performed on fibroblasts cultured on polypropylene mesh with nanofibrous membrane (PP + NM) compared to those grown on standard cell culture plates. Principal component analysis (**A**). Volcano plot of differentially expressed genes (**B**). Gene ontology (GO) enrichment analysis of differentially expressed genes (**C**). Heatmap of differentially expressed genes of interest (**D**-**F**). KEGG analysis of differentially expressed genes (**G**). Gene set enrichment analysis (GSEA) of gene sets identified from GO and KEGG analysis (**H**)

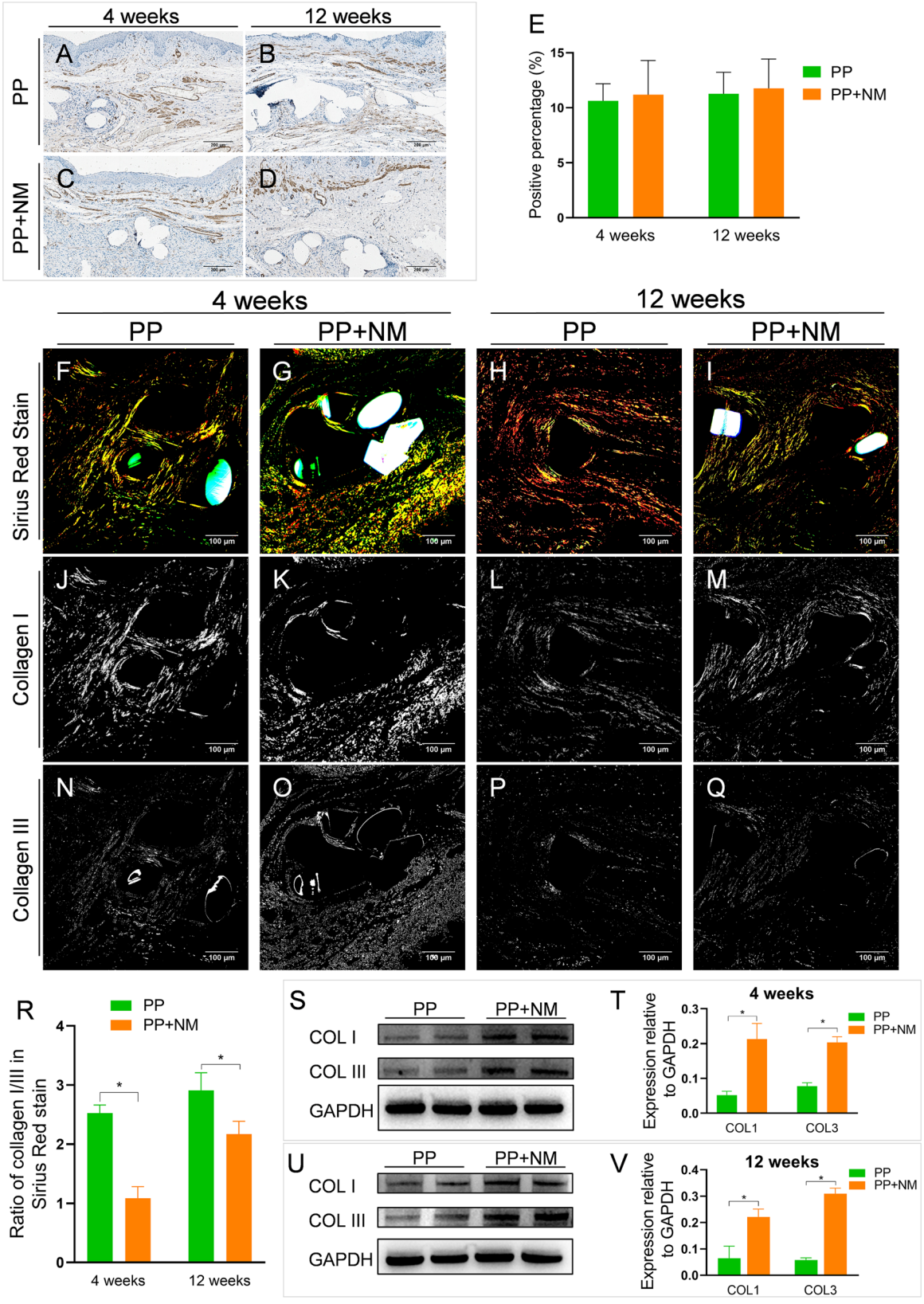

Fig. 5 Evaluation of smooth muscle fibers and collagen deposition in vaginal wall tissues of rats. Immunohistochemistry (IHC) staining of ACTA2 (**A**-**D**) and the positive area percentage analyzing (**E**). Picro-Sirius red staining for vaginal wall tissues (**F**-**Q**). Analysis of the collagen I to III ratio (**R**). Western blotting quantitative analysis of the expression of type I and type III collagen in tissues at 4 weeks (**S**-**T**) and 12 weeks (**U**-**V**). Scale bars in A-D are 200um. Scale bars in F-Q are 100um. * indicates $P < 0.05$

revealed no significant difference in ACTA2 IHC-positive area between two groups at both 4 weeks and 12 weeks (Fig. 5E. $P=0.793$ and 0.801, respectively).

Changes in collagen composition and content

As depicted in Fig. 5F-Q, the ratio of collagen I to III was assessed using Picro-Sirius red staining. At both 4 weeks and 12 weeks, the PP group demonstrated a significantly higher ratio compared to the PP+NM group (Fig. 5R, $P<0.001$ and $=0.025$, respectively). Western blotting analysis revealed that the expression levels of collagen I and III of PP group were significantly lower than that of PP + NM group at 4 weeks (Fig. 5S-T, $P<0.001$ and $=0.007$, respectively). Similarly, at 12 weeks post implantation, there was a significant decrease in the expression of collagen I and III proteins in PP group (Fig. 5U-V, $P<0.001$ and <0.001, respectively).

Changes in enzymes related to collagen deposition

The expression levels of MMPs reflected the catabolism of the extracellular matrix in tissues, while the expression levels of TIMPs indicated the extent of inhibition on this catabolism process. As shown in Fig. 6A-P, the staining intensity of TIMP1 and TIMP2 was comparatively lighter in the PP group, while MMP2 and MMP9 exhibited deeper staining, indicating enhanced collagen catabolism in the PP group. This consistent finding was evident at both 4 and 12 weeks. The quantitative analysis of IHC was presented in Fig. 6Q-R. At 4 weeks, the expression levels of TIMP1 and TIMP2 were significantly lower in the PP group (Fig. 6Q, $P=0.006$ and 0.031, respectively). Additionally, MMP2 and MMP9 expression was down-regulated in the PP+NM group at 4 weeks (Fig. 6Q, $P=0.023$ and 0.013, respectively). Similar results were observed at 12 weeks with lower expression levels of TIMP1 and TIMP2 in the PP group (Fig. 6R, $P=0.017$ and 0.011, respectively), as well as lower expression levels of MMP2 and MMP9 in the PP+NM group (Fig. 6Q, $P=0.011$ and 0.005, respectively). The Western blotting assays confirmed the IHC results. At 4 weeks, the expression levels of TIMP1 and TIMP2 were significantly decreased in the PP group (Fig. 6S-T, $P<0.001$ and $=0.022$, respectively), whereas the expression levels of MMP2 and MMP9 were significantly increased in the PP group (Fig. 6T, $P=0.024$ and 0.014, respectively). At 12 weeks, TIMP1 and TIMP2 expression levels were down-regulated in the PP group (Fig. 6U-V, $P=0.018$ and 0.012, respectively), whereas an up-regulation of MMP2 and MMP9 expression was observed in the PP group (Fig. 6V, $P=0.012$ and 0.006, respectively).

Activation of the TGF-β1/Smad3/p38/ERK1/2 signaling pathway

TGF-β1, Smad3, p38, and ERK1/2 were the main proteins in ECM regulation-related signaling pathways. Western blotting was conducted to assess the expression or phosphorylation levels of these proteins (Fig. 7A). Quantitative analysis was also performed. As depicted in Fig. 7B-C, the expression of TGF-β1 was significantly up-regulated in the PP+NM group at both 4 and 12 weeks ($P<0.001$ and $=0.002$, respectively). The phosphorylation level of Smad3, p38, and ERK1/2 exhibited an increase in PP+NM group at 4 weeks ($P<0.001$, $=0.009$, and 0.004, respectively). Similarly, at 12 weeks, there was an increase in the phosphorylation levels of Smad3, p38, and ERK1/2 in the PP+NM group, as shown in ($P=0.011$, 0.009, and $=0.010$, respectively). Western blotting assays also showed no significant changes in ATCA2 between both groups at either time point (Fig. 7B-C, $P=0.860$ and 0.695, respectively).

Evaluation of microvascular density

Through vWF staining (Fig. 7D-G), it was observed that the PP+NM group exhibited a significantly higher microvascular density compared to the PP group at both the 4 and 12 weeks. Given that the results were readily discernible from the images, we opted not to conduct a quantitative analysis. This suggests that, in comparison to PP mesh, PP+NM is advantageous for promoting neovascularization.

Evaluation of macrophage recruiting and TNF-α expression

The recruitment of macrophages and the elevated expression of TNF-α are critical indicators of foreign body reaction associated with the implanted mesh. IHC staining for F4/80 revealed that the number of F4/80-positive cells around the implanted mesh fiber in the PP+NM group was significantly lower than that in the PP group at both 4 weeks and 12 weeks (Fig. 7H-K). Additionally, TNF-α expression in the PP+NM group was markedly reduced compared to that in the PP group at both time points (Fig. 7L-O). Given the visual differences observed, quantitative analysis was omitted. These findings suggested that NM-coated mesh can substantially mitigate the foreign body response elicited by PP mesh.

Discussion

In this study, a co-axial electrospun nanofibrous membrane was fabricated and coated on a PP mesh, and the electrospun fibers were composed of polyurethane as the fibers' core and gelatin as the fibers' shell. The composite mesh (PP+NM) inhibited the catabolism of extracellular matrix both in vitro and in vivo. In a POP rat model, the complications associated with PP mesh implantation were significantly reduced by the modified PP mesh.

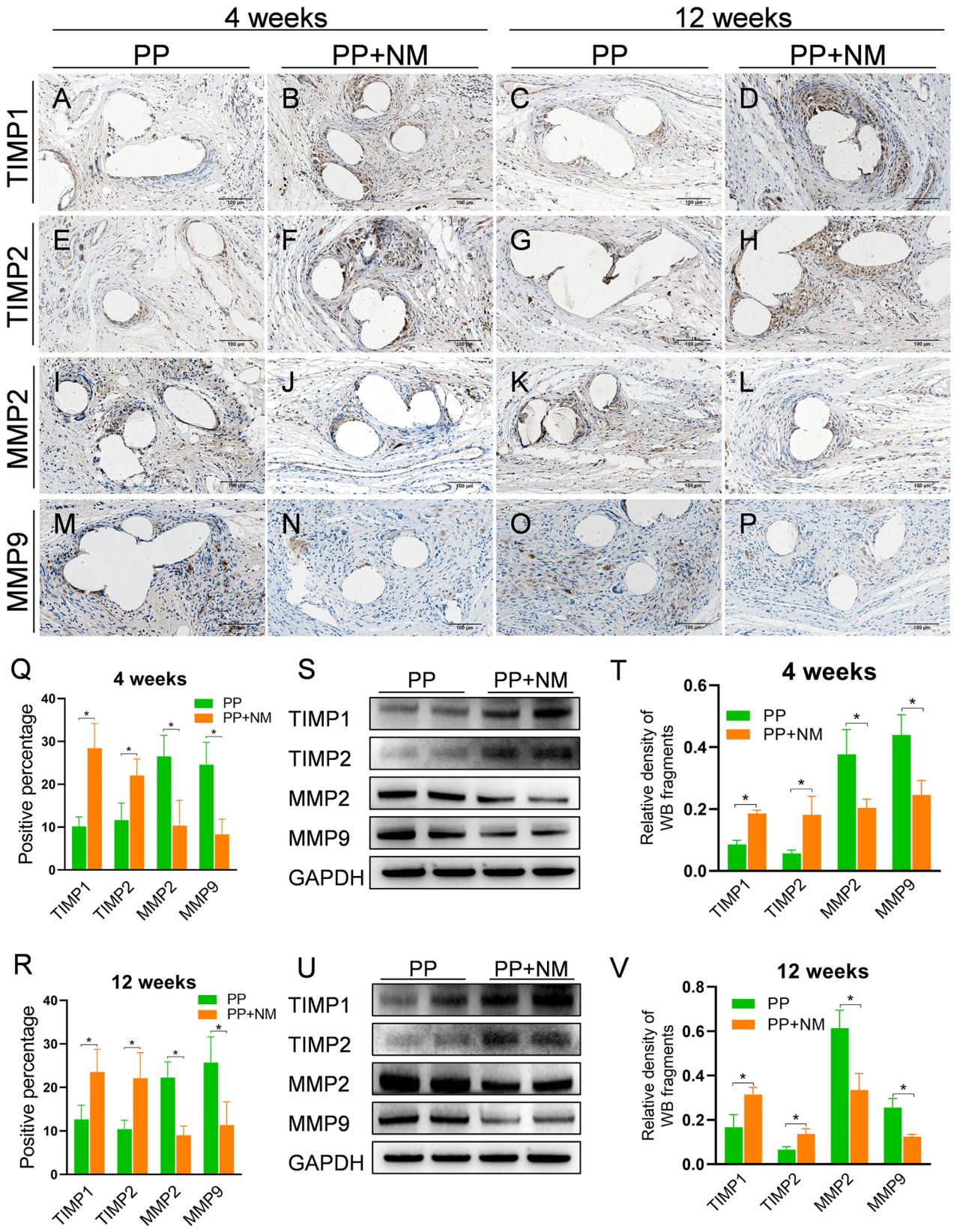

Fig. 6 Evaluation on the expression of enzymes related to collagen deposition in vivo. Immunohistochemistry (IHC) staining for TIMP1 (**A**-**D**), TIMP2 (**E**-**H**), MMP2 (**I**-**L**), and MMP9 (**M**-**P**) in vaginal wall tissues of rats. Positive area percentage of IHC was analyzed and compared among groups (**Q**-**R**). Western blotting quantitative analysis of the expression of TIMPs and MMPs in tissues at 4 weeks (**S**-**T**) and 12 weeks (**U**-**V**). Scale bars in A-P were 100um. * indicates $P < 0.05$

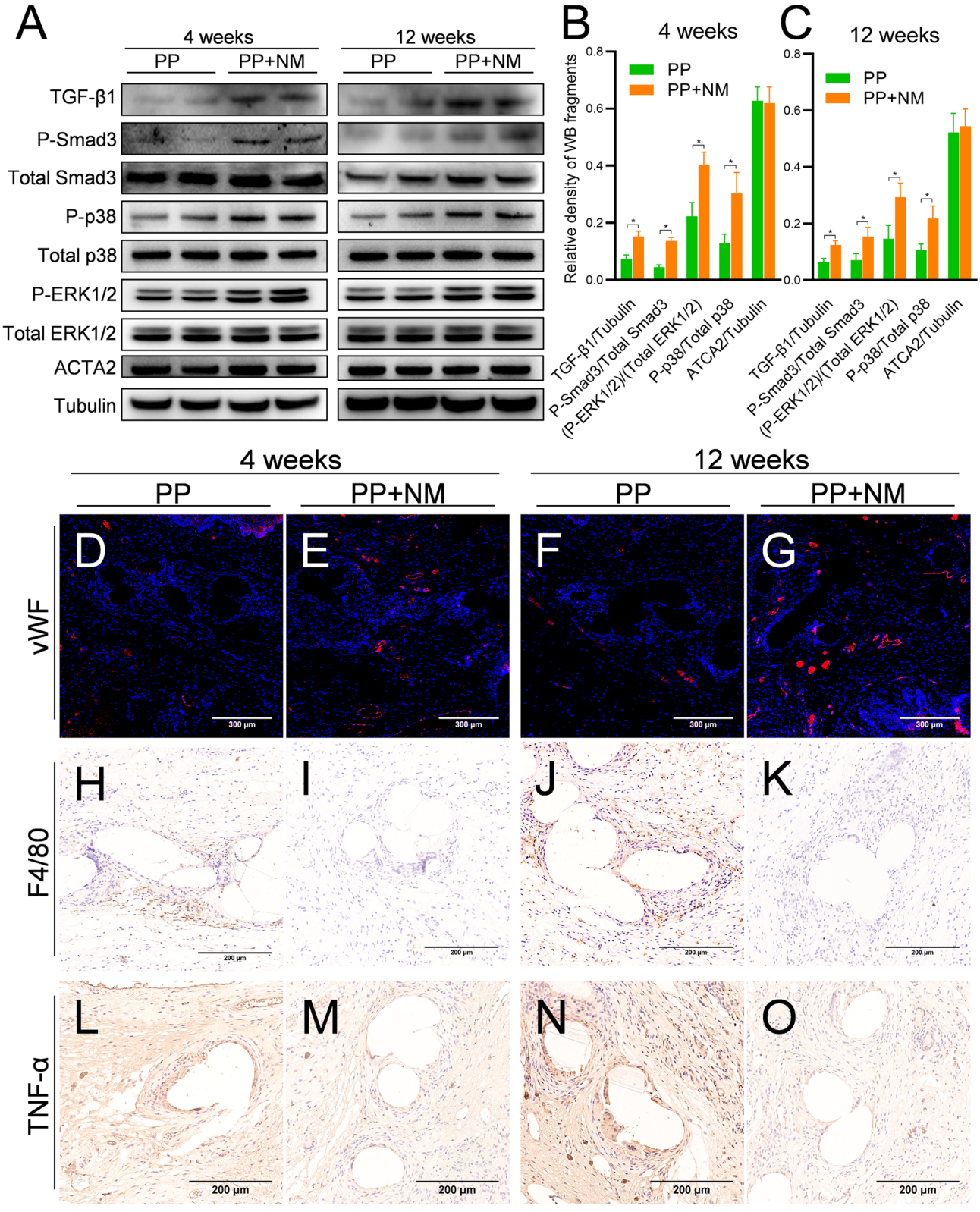

Fig. 7 Evaluation on the activation of associated signaling pathway and the biocompatibility of nanofibrous membrane. Western blotting assays for the expression TGF-β1, P-Smad3, total Smad2, P-p38, total p38, P-ERK1/2, total ERK1/2, and tubulin as a reference in vaginal wall tissues of rats at 4 and 12 weeks (**A**). Western blotting quantitative analysis of the protein expression at 4 weeks (**B**) and 12 weeks (**C**). IF staining of the vWF for evaluating microvascular density (**D**-**G**). IHC staining of the F4/80 (**H**-**K**) and TNF-α (**L**-**O**) for evaluating macrophage recruitment and foreign body reaction. Scale bars in D-G were 300um. Scale bars in H-O were 200um. * indicates $P < 0.05$

The high stiffness of PP is largely different from that of the surrounding natural tissue, which is a crucial factor that induceds foreign body reactions that contribute to the complications associated with the PP mesh [11]. The high stiffness of PP is likely to result in a disproportionate distribution of stress between the mesh and adjacent tissues [23].

Studies have demonstrated that transvaginal implantation of PP mesh leads to shrinkage due to excessive stress, which triggers fibrous tissue formation around the mesh [24], whereas inadequate stress loading in the neighboring native tissues causes degradation of extracellular matrix, leading to erosion and exposure of the mesh to vaginal mucosa [25]. This phenomenon is referred to as "stress shielding".

In addition, implantation of the mesh induces a foreign body reaction which can be elicited by mismatched mechanical properties as well as by the low biocompatibility of implanted medical devices or biomaterials. It is documented that the Young's modulus of PP is about 4.5 N/mm^2, and polyurethane is about 1–2 N/mm^2 that is closer to the mechanical properties of native tissues. Moreover, after dynamic loading for 7 days, PP increased in stiffness and showed plastic deformation while polyurethane remained elastic [26]. Consequently, this can lead to an increase in aseptic inflammation surrounding the mesh. Aseptic inflammation exacerbates the degradation of the extracellular matrix. The foreign body reaction eventually manifested as pathological fibrosis formation of the mesh body and degradation of extracellular matrix in the native vaginal wall tissue surrounding the mesh, thus promoting the occurrence of mesh complications [27].

In this study, the nanofibrous membrane was prepared from gelatin and polyurethane. These two materials are commonly used in the preparation of biological implants and have shown good biocompatibility in previous studies [15, 16]. Gelatin is derived from the degradation of collagen in biological tissue that is a biocompatible and easily degradable with excellent water retention properties. Consequently, it finds extensive applications in various fields especially in wound healing [14, 28]. However, gelatin is of poor mechanical properties and structural stability [29]. In this study, gelatin was used as the fibers' shell to provide biocompatibility and polyurethane was employed as the core to provide suitable mechanical supporting. PU was not biodegradable. As for the gelatin, it is biodegradable, and its degradation in vivo is mainly caused by proteases. When used as a single material, gelatin decomposes completely within 3 h at its maximum rate. While the presence of PU in electrospun nanofibers significantly enhanced its degradation resistance up to 14 days, which is much in line with the process for tissue regeneration [30].

A study by Rebecca et al. revealed that structural alterations in smooth muscle fibers within the vaginal wall caused by PP mesh could be the cause of complications [31]. In this study, there were no significant changes observed in the expression of smooth muscle between two groups. However, disruption of smooth muscle fiber morphology was evident in the PP group. Consequently, it is hypothesized that the mechanism underlying the reduction of mesh-related complications may involve the stabilization of the smooth muscle layer by PP+NM, rather than an enhancement in the quantity of smooth muscle fibers.

The two primary parameters of interest in POP disease are tissue strength and tissue elasticity. A decrease in the total amount of collagen leads to a decrease in tissue strength [32]. The increased ratio of type I to type III collagen can lead to decreased tissue elasticity [33]. The presence of these two histological features directly contributes to the development of complications following mesh implantation [34]. In this study, the potential of NM to ameliorate mesh-related complications by modulating collagen metabolism may be manifested in two aspects. Firstly, NM demonstrated an ability to enhance collagen deposition in both in vitro and in vivo experiments, thereby augmenting the total collagen content in tissues and preserving tissue integrity. Secondly, NM decreased the ratio of type I to type III collagen, contributing to the maintenance of tissue elasticity. The main component of extracellular matrix in vaginal wall tissue is collagen. MMPs promotes collagen catabolism while TIMPs inhibits it. Previous studies have shown that MMPs expression is elevated and TIMPs expression is decreased in tissue implanted with mesh [11, 34]. The increasing in collagen catabolism ultimately leads to tissue weakness. In this study, the up-regulation of TIMPs and down-regulation of MMPs was observed in both in vitro and in vivo experiments. The comprehensive effect of the modified mesh on collagen was the inhibition of catabolism in both in vitro and in vivo experiments. In addition, ATCA2 expression did not show significant differences regulated by NM. The expression of ATCA2 is an important marker for the differentiation of fibroblasts into myofibroblasts. This suggested that the regulation of collagen metabolism might not be achieved through the mediation of fibroblasts differentiation. The deposition of collagen may be mediated through the activation of the TGF-β1/Smad3/p38/ERK signaling pathway, as supported by our mRNA sequencing and in vivo findings. However, this study did not focus on the specific mechanisms of collagen metabolism regulated by NM. Further research is warranted to substantiate this hypothesis.

In this study, the PP+NM group exhibited a significant reduction in the number of macrophages surrounding the implanted mesh. Previous research had confirmed

that foreign body reaction characterized by macrophage recruitment was one of the causes of complications associated with PP mesh [35]. The expression level of TNF-α around the PP mesh fibers, which reflected the degree of local sterile inflammatory response in the tissue [36], was significantly lower in the PP+NM group. Furthermore, we observed a higher microvascular density around the mesh fiber in the PP+NM group, which was closely related to tissue repair. Taken together, these three findings suggested that NM markedly enhanced the biocompatibility of PP mesh.

The strengths of this study were as follows. Firstly, PP mesh has been in clinical use for a long time and has obvious advantages in anatomical restoration and reducing recurrence. This modification enabled the mesh preserve these advantages while effectively mitigating potential complications. Secondly, the surface area of the PP mesh is insufficient for drug or cell loading. The nanofibrous membrane provided a more suitable substrate for the cellular growth. Besides, local administration of estrogen has been reported to mitigate complications associated with mesh implants. In future investigations, this nanofibrous membrane could be explored as a potential carrier for delivering estrogen or other therapeutic agents, in addition, nanofibrous membranes may serve as carriers to facilitate cell delivery.

The limitations of this study were as follows: Firstly, the size of the POP model developed in rats was relatively small, which restricted the implantation of meshes of the size equal to the commonly used in clinical settings. Therefore, it is necessary to conduct further testing on large animal models and even primates prior to initiating clinical trials. Another limitation lies in our utilization of only one formulation for the nanofiber membrane. Considering that different formulations can significantly influence the characteristics of nanofibers, explorations on various formulations should be conducted in the future.

Conclusions

In conclusion, the PP mesh modified with nanofibrous membrane prepared by co-axial electrospinning technique effectively reduced mesh related complications in a POP rat model. The implanted modified mesh inhibited the catabolism of collagen in the tissues surrounding the mesh by regulating the TGF-β1/Smad3/p38/ERK signaling pathway. This strategy holds promising prospects for the treatment of pelvic organ prolapse.

Abbreviations

ACTA2	Alpha smooth muscle actin
COL	Collagen
ERK	Extracellular signal-regulated kinases
GAPDH	Reduced glyceraldehyde-phosphate dehydrogenase
HE	Simulated vaginal delivery
LSC	Laparoscopic sacrocolpopexy
MMP	Matrix metalloproteinase
NM	Nanofibrous membrane
NTR	Native tissue repair
OVX	Ovariectomy
POP	Pelvic organ prolapse
PP	Polypropylene
PU	Polyurethane
Smad	Mothers against decapentaplegic
SVD	Simulated vaginal delivery
TGF	Transforming growth factor
TIMP	Tissue inhibitor of metalloproteinase
TVM	Transvaginal mesh

Acknowledgements

Thanks for the support from the National Science and Technology Key Infrastructure on Translational Medicine in Peking Union Medical College Hospital.

Author contributions

T.G: conceptualization, data curation, methodology, software, manuscript writing and revision. XC.H, Z.D, XQ.W: data curation, methodology, validation. JH.L, J.L: conceptualization, project administration, supervision, manuscript reviewing and revision. HY.X, ZJ.S: conceptualization, methodology, project administration, funding acquisition, manuscript reviewing and revision. All authors read and approved the final manuscript.

Funding

This research was funded by the National Natural Science Foundation of China (81971366); Beijing Natural Science Foundation (grant numbers: L232124); Capital Foundation of Medical Development (grant numbers: 2024-2-4014); and Chinese Academy of Medical Sciences (CAMS) Innovation Fund for Medical Sciences (grant numbers: 2023-I2M-C&T-B-033).

Data availability

All data generated or analysed during this study are included in this published article.

Declarations

Ethics approval and consent to participate

This study protocol was approved by the ethics committee of Peking Union Medical College Hospital (no. JS-2240, 25/02/2020). Written informed consent was obtained from the participants.

Consent for publication

Not applicable.

Competing interests

The authors declare no competing interests.

Author details

[1]Department of Obstetrics and Gynecology, Peking Union Medical College Hospital, Chinese Academy of Medical Sciences and Peking Union Medical College, National Clinical Research Center for Obstetric & Gynecologic Diseases, No. 1 Shuaifuyuan, Dongcheng District, Beijing, China
[2]Institute of Basic Medical Sciences, Chinese Academy of Medical Sciences and Peking Union Medical College, Beijing 100005, China
[3]State Key Laboratory of Advanced Medical Materials and Devices, Tianjin Institutes of Health Science, Chinese Academy of Medical Science & Peking Union Medical College, Tianjin 300192, China

Received: 16 June 2024 / Accepted: 25 September 2024
Published online: 03 October 2024

References

1. Wu JM, Matthews CA, Conover MM, Pate V, Jonsson Funk M. Lifetime risk of stress urinary incontinence or pelvic organ prolapse surgery. Obstet Gynecol. 2014;123(6):1201–6. https://doi.org/10.1097/aog.0000000000000286

2. Fialkow MF, Newton KM, Lentz GM, Weiss NS. Lifetime risk of surgical management for pelvic organ prolapse or urinary incontinence. Int Urogynecol J Pelvic Floor Dysfunct. 2008;19(3):437–40. https://doi.org/10.1007/s00192-007-0459-9
3. Altman D, Väyrynen T, Engh ME, Axelsen S, Falconer C. Anterior colporrhaphy versus transvaginal mesh for pelvic-organ prolapse. N Engl J Med. 2011;364(19):1826–36. https://doi.org/10.1056/NEJMoa1009521
4. Capobianco G, Sechi I, Muresu N, Saderi L, Piana A, Farina M, Dessole F, Virdis G, De Vita D, Madonia M, Petrillo M, Sotgiu G. Native tissue repair (NTR) versus transvaginal mesh interventions for the treatment of anterior vaginal prolapse: systematic review and meta-analysis. Maturitas. 2022;165:104–12. https://doi.org/10.1016/j.maturitas.2022.07.013
5. Glazener CM, Breeman S, Elders A, Hemming C, Cooper KG, Freeman RM, Smith AR, Reid F, Hagen S, Montgomery I, Kilonzo M, Boyers D, McDonald A, McPherson G, MacLennan G, Norrie J. Mesh, graft, or standard repair for women having primary transvaginal anterior or posterior compartment prolapse surgery: two parallel-group, multicentre, randomised, controlled trials (PROSPECT). Lancet (London England). 2017;389(10067):381–92. https://doi.org/10.1016/s0140-6736(16)31596-3
6. Morling JR, McAllister DA, Agur W, Fischbacher CM, Glazener CM, Guerrero K, Hopkins L, Wood R. Adverse events after first, single, mesh and non-mesh surgical procedures for stress urinary incontinence and pelvic organ prolapse in Scotland, 1997–2016: a population-based cohort study. Lancet (London England). 2017;389(10069):629–40. https://doi.org/10.1016/s0140-6736(16)32572-7
7. Ugianskiene A, Davila GW, Su TH. FIGO review of statements on use of synthetic mesh for pelvic organ prolapse and stress urinary incontinence. Int J Gynaecol Obstet. 2019;147(2):147–55. https://doi.org/10.1002/ijgo.12932
8. Ding J, Deng M, Song XC, Chen C, Lai KL, Wang GS, Yuan YY, Xu T, Zhu L. Nanofibrous biomimetic mesh can be used for pelvic reconstructive surgery: a randomized study. J Mech Behav Biomed Mater. 2016;61:26–35. https://doi.org/10.1016/j.jmbbm.2016.01.003
9. Lu Y, Dong S, Zhang P, Liu X, Wang X. Preparation of a polylactic acid knitting mesh for pelvic floor repair and in vivo evaluation. J Mech Behav Biomed Mater. 2017;74:204–13. https://doi.org/10.1016/j.jmbbm.2017.05.034
10. Roman S, Urbánková I, Callewaert G, Lesage F, Hillary C, Osman NI, Chapple CR, Deprest J, MacNeil S. Evaluating alternative materials for the treatment of stress urinary incontinence and pelvic organ prolapse: a comparison of the in vivo response to meshes implanted in rabbits. J Urol. 2016;196(1):261–9. https://doi.org/10.1016/j.juro.2016.02.067
11. Abhari RE, Izett-Kay ML, Morris HL, Cartwright R, Snelling SJB. Host-biomaterial interactions in mesh complications after pelvic floor reconstructive surgery. Nat Reviews Urol. 2021;18(12):725–38. https://doi.org/10.1038/s41585-021-00511-y
12. Gargett CE, Gurung S, Darzi S, Werkmeister JA, Mukherjee S. Tissue engineering approaches for treating pelvic organ prolapse using a novel source of stem/stromal cells and new materials. Curr Opin Urol. 2019;29(4):450–7. https://doi.org/10.1097/mou.0000000000000634
13. Boennelycke M, Gras S, Lose G. Tissue engineering as a potential alternative or adjunct to surgical reconstruction in treating pelvic organ prolapse. Int Urogynecol J. 2013;24(5):741–7. https://doi.org/10.1007/s00192-012-1927-4
14. Mogoşanu GD, Grumezescu AM. Natural and synthetic polymers for wounds and burns dressing. Int J Pharm. 2014;463(2):127–36. https://doi.org/10.1016/j.ijpharm.2013.12.015
15. Ranakoti L, Gangil B, Bhandari P, Singh T, Sharma S, Singh J, Singh S. Promising role of polylactic acid as an ingenious biomaterial in scaffolds, drug delivery, tissue engineering, and medical implants: research developments, and prospective applications. Molecules. 2023;28(2). https://doi.org/10.3390/molecules28020485
16. Zahran M, Marei AH. Innovative natural polymer metal nanocomposites and their antimicrobial activity. Int J Biol Macromol. 2019;136:586–96. https://doi.org/10.1016/j.ijbiomac.2019.06.114
17. Yoon J, Yang HS, Lee BS, Yu WR. Recent progress in coaxial electrospinning: new parameters, various structures, and wide applications. Adv Mater. 2018;30(42):e1704765. https://doi.org/10.1002/adma.201704765
18. Sill TJ, von Recum HA. Electrospinning: applications in drug delivery and tissue engineering. Biomaterials. 2008;29(13):1989–2006. https://doi.org/10.1016/j.biomaterials.2008.01.011
19. Guo T, Du Z, Wang XQ, Lang JH, Sun ZJ. Ovariectomy with simulated vaginal delivery to establish a rat model for pelvic organ prolapse. Connect Tissue Res. 2023;64(4):376–88. https://doi.org/10.1080/03008207.2023.2199091
20. Tang D, Chen M, Huang X, Zhang G, Zeng L, Zhang G, Wu S, Wang Y. SRplot: a free online platform for data visualization and graphing. PLoS ONE. 2023;18(11):e0294236. https://doi.org/10.1371/journal.pone.0294236
21. Farr NTH, Roman S, Schäfer J, Quade A, Lester D, Hearnden V, MacNeil S, Rodenburg C. A novel characterisation approach to reveal the mechano-chemical effects of oxidation and dynamic distension on polypropylene surgical mesh. RSC Adv. 2021;11(55):34710–23. https://doi.org/10.1039/d1ra05944k
22. Haylen BT, Freeman RM, Swift SE, Cosson M, Davila GW, Deprest J, Dwyer PL, Fatton B, Kocjancic E, Lee J, Maher C, Petri E, Rizk DE, Sand PK, Schaer GN, Webb RJ. An International Urogynecological Association (IUGA) / International Continence Society (ICS) joint terminology and classification of the complications related directly to the insertion of prostheses (meshes, implants, tapes) & grafts in female pelvic floor surgery. Int Urogynecol J. 2011;22(1):3–15. https://doi.org/10.1007/s00192-010-1324-9
23. Sumner DR, Galante JO. Determinants of stress shielding: design versus materials versus interface. Clin Orthop Relat Res. 1992;274:202–12.
24. Tennyson L, Rytel M, Palcsey S, Meyn L, Liang R, Moalli P. Characterization of the T-cell response to polypropylene mesh in women with complications. Am J Obstet Gynecol. 2019;220(2):187e. https://doi.org/10.1016/j.ajog.2018.11.121
25. Liang R, Abramowitch S, Knight K, Palcsey S, Nolfi A, Feola A, Stein S, Moalli PA. Vaginal degeneration following implantation of synthetic mesh with increased stiffness. BJOG. 2013;120(2):233–43. https://doi.org/10.1111/1471-0528.12085
26. Hillary CJ, Roman S, Bullock AJ, Green NH, Chapple CR, MacNeil S. Developing repair materials for stress urinary incontinence to withstand dynamic distension. PLoS ONE. 2016;11(3):e0149971. https://doi.org/10.1371/journal.pone.0149971
27. Knight KM, King GE, Palcsey SL, Suda A, Liang R, Moalli PA. Mesh deformation: a mechanism underlying polypropylene prolapse mesh complications in vivo. Acta Biomater. 2022;148:323–35. https://doi.org/10.1016/j.actbio.2022.05.051
28. Li T, Sun M, Wu S. State-of-the-art review of electrospun gelatin-based nanofiber dressings for wound healing applications. Nanomaterials (Basel Switzerland). 2022;12(5). https://doi.org/10.3390/nano12050784
29. Gomes SR, Rodrigues G, Martins GG, Roberto MA, Mafra M, Henriques CM, Silva JC. In vitro and in vivo evaluation of electrospun nanofibers of PCL, chitosan and gelatin: a comparative study. Mater Sci Eng C Mater Biol Appl. 2015;46:348–58. https://doi.org/10.1016/j.msec.2014.10.051
30. Sheikholeslam M, Wright MEE, Cheng N, Oh HH, Wang Y, Datu AK, Santerre JP, Amini-Nik S, Jeschke MG. Electrospun polyurethane-gelatin composite: a new tissue-engineered scaffold for application in skin regeneration and repair of complex wounds. ACS Biomater Sci Eng. 2020;6(1):505–16. https://doi.org/10.1021/acsbiomaterials.9b00861
31. Shaffer RM, Liang R, Knight K, Carter-Brooks CM, Abramowitch S, Moalli PA. Impact of polypropylene prolapse mesh on vaginal smooth muscle in rhesus macaque. Am J Obstet Gynecol. 2019;221(4):330e. https://doi.org/10.1016/j.ajog.2019.05.008
32. Zhu YP, Ting X, Tao G, Jing SZ. Lang Jing he %J International Urogynecology Journal: evaluation of extracellular matrix protein expression and apoptosis in the uterosacral ligaments of patients with or without pelvic organ prolapse. 2020;6.
33. Xue M, Jackson CJ. Extracellular matrix reorganization during wound healing and its impact on abnormal scarring. Adv Wound Care (New Rochelle). 2015;4(3):119–36. https://doi.org/10.1089/wound.2013.0485
34. Darzi S, Urbankova I, Su K, White J, Lo C, Alexander D, Werkmeister JA, Gargett CE, Deprest J. Tissue response to collagen containing polypropylene meshes in an ovine vaginal repair model. Acta Biomater. 2016;39:114–23. https://doi.org/10.1016/j.actbio.2016.05.010
35. Brown BN, Mani D, Nolfi AL, Liang R, Abramowitch SD, Moalli PA. Characterization of the host inflammatory response following implantation of prolapse mesh in rhesus macaque. Am J Obstet Gynecol. 2015;213(5):668. https://doi.org/10.1016/j.ajog.2015.08.002

36. Lo TS, Lin YH, Yusoff FM, Chu HC, Hsieh WC, Uy-Patrimonio MC. The immunohistochemical and urodynamic evaluation towards the collagen-coated and non-coated polypropylene meshes implanted in the pelvic wall of the rats. Sci Rep. 2016;6:38960. https://doi.org/10.1038/srep38960

Publisher's note